Enhanced weathering leads to substantial C accrual on crop macrocosms

Francois Rineau*[1], Alexander H. Frank[2,3], Jannis Groh[4,5,6], Kristof Grosjean[1], Arnaud Legout[7], Daniil I. Kolokolov[8], Michel Mench[9], Maria Moreno-Druet[1], Benoît Pollier[7], Virmantas Povilaitis[10], Johanna Pausch[11], Thomas Puetz[5], Tjalling Rooks[1], Peter Schröder[12], Wieslaw Szulc[13], Beata Rutkowska[13], Xander Swinnen[1], Sofie Thijs[1], Harry Vereecken[5], Janna V. Veselovskaya[8], Mwahija Zubery[1], Renaldas Žydelis[10], Evelin Loit[14]

[1]Environmental Biology, Centre for Environmental Sciences, Hasselt University, Diepenbeek, Belgium.
[2]Center of Stable Isotope Research in Ecology and Biogeochemistry (BayCenSI), BayCEER, University of Bayreuth, Universitätsstr. 30, 95445 Bayreuth, Germany
[3]Department of Plankton and Microbial Ecology, Leibniz Institute of Freshwater Ecology and Inland Fisheries (IGB), Zur alten Fischerhütte 2, 16775 Stechlin, Germany
[4]Department of Soil Science and Soil Ecology, Institute of Crop Science and Resource Conservation, University of Bonn, Bonn, Germany
[5]Agrosphere Institute (IBG-3), Forschungszentrum Jülich (FZJ), Jülich, Germany
[6]Isotope Biogeochemistry and Gas Fluxes, Research Area 1 "Landscape Functioning", Leibniz Centre for Agricultural Landscape Research (ZALF), Müncheberg, Germany
[7]INRAE, BEF, F-54000 Nancy, France
[8]Boreskov Institute of Catalysis, Novosibirsk, Ac. Lavrentiev av. 5, Novosibirsk 630090, Russia
[9]Univ. Bordeaux, INRAE, Biogeco, Bat B2, Allée G. St-Hilaire, F-33615 Pessac cedex, France
[10]Institute of Agriculture, Lithuanian Research Centre for Agriculture and Forestry, Lithuania
[11]Agroecology, BayCEER, University of Bayreuth, Universitätsstr. 30, 95445 Bayreuth, Germany
[12]Helmholtz Center Munich, Research Unit Environmental Simulation, Ingolstädter Landstrasse 1, D-85764 Neuherberg
[13]Institute of Agriculture, Warsaw University of Life Sciences, Nowoursynowska 166, 02-787 Warsaw, Poland
[14]Estonian Univ Life Sci, Inst Agr & Environm Sci, Tartu, Estonia

Correspondence to: François Rineau (francois.rineau@uhasselt.be)

Abstract. Enhanced weathering (EW) is proposed as a key strategy for climate change mitigation and carbon dioxide removal technology. Dissolution of silicate minerals enhances the alkalinity of the pore water, resulting at a shift of the carbonate system towards carbonate and bicarbonate, leading to higher dissolved inorganic carbon when the water is equilibrated with the atmosphere. Here, we evaluated the effects of EW on a crop ecosystem under future climate change conditions within a macro-scale ecotron—an enclosed facility enabling complete quantification of carbon fluxes among the atmosphere, vegetation, soil, and leachates. We monitored all greenhouse gases in deep mesocosms representative of marginal soil conditions and, after liming and fertilization, applied 10 t ha^{-1} of basalt at the start of the experiment. EW treatment resulted in an almost three-fold enhancement of measured carbon flux into the soil, achieving rates up to 1.5 tons per hectare during the growing season. Moreover, the observed carbon sequestration surpassed the levels expected from weathering processes alone. This is notable because the near-neutral soil pH environment was not favourable to EW kinetics. . Therefore, we conclude that EW facilitated significant carbon accrual in our simulated ecosystems via not only carbonate precipitation but also enhanced biogeochemical activities promoting additional carbon storage. Based on these findings, we speculate on the underlying pathways responsible for such outcomes.

1 Introduction

Enhanced rock weathering (EW) has emerged as a promising negative emissions strategy and carbon dioxide removal (CDR) approach, specifically aimed at achieving a net negative greenhouse gas balance in the near future and reducing carbon emissions from the agricultural sector (Beerling et al., 2020). The method involves applying silicate rock dust to soils, where the dissolution of silicate minerals increases the alkalinity of pore water, shifting the carbonate system toward carbonate and bicarbonate ions and leading to higher dissolved inorganic carbon when the water equilibrates with the atmosphere. Theoretically, these carbonates may either remain in the soil or be leached into groundwater and transported to aquatic systems, where they could help reduce ocean acidification—both pathways contributing to carbon sequestration. Early studies support some of these theoretical predictions (Dietzen & Rosing, 2023; Guo et al., 2023; Rijnders et al., 2023), suggesting that EW could be implemented across large agricultural areas. Its carbon removal potential is estimated at 0.5 to 4 Gt CO_2 per year (Beerling et al., 2020), with additional benefits for soil health in nutrient-poor soils (Beerling et al., 2018). However, significant uncertainties remain—particularly for agricultural soils (Cipolla et al., 2021)—underscoring the need for robust experimental validation. Assessing the net impact of enhanced silicate weathering on soil carbon budgets is for example complicated by the tight coupling between organic and inorganic carbon dynamics. On the one hand, silicate dissolution contributes to inorganic C sequestration through carbonate precipitation and organo-mineral associations, such as stimulation of mineral -associated

organic matter (Xu et al., 2024). On the other, it indirectly influences the largest terrestrial C pool—soil organic carbon—via changes in nutrient availability, microbial activity, litter quality, and aggregate formation. These processes can either promote stabilization of organic matter or accelerate its mineralization, with outcomes that vary across timescales and soil types (Vicca et al., 2022). In addition, secondary mineral formation (e.g. clays, Fe/Al (hydr)oxides, or pedogenic carbonates) can reduce DIC availability for export while providing new sorption surfaces that affect soil organic C stabilization.

While enhanced weathering is typically framed in terms of inorganic CO_2 sequestration through pedogenic carbonate formation or leaching of dissolved weathering products, these fluxes can be relatively minor compared to other soil C processes. A substantial fraction of released base cations may instead be retained on exchange sites or incorporated into secondary minerals such as clays or Fe/Al (hydr)oxides, thereby bypassing direct CO_2 uptake. Moreover, organic carbon fluxes often exceed inorganic fluxes by orders of magnitude, with soil organic matter decomposition potentially releasing far more CO_2 than is sequestered via mineral weathering. At the same time, silicate amendments can enhance plant productivity and promote the transfer of organic C into more stable soil fractions through aggregation and mineral associations (Vienne et al., 2024). These contrasting effects illustrate the difficulty of isolating a single mechanism and highlight the need for integrative approaches that jointly consider inorganic sinks, organic matter dynamics, and secondary mineral formation when evaluating the true CO_2 removal potential of enhanced weathering (Steinwidder et al., 2025). Together, these processes illustrate that reliable estimates of carbon dioxide removal (CDR) through enhanced weathering must account for both inorganic and organic C pools, as well as the role of secondary mineral phases, rather than focusing solely on weathering rates.

To address these limitations, we conducted an EW amendment experiment under future climate change conditions on an artificially marginalized land that has been subjected to fertilization and cropping, within an ecotron—a controlled, closed-environment facility that enables real-time monitoring of ecosystem-level carbon fluxes (Roy et al., 2021). This enabled us to close the carbon mass balance in the system and to study the fate of released cations, while the large macrocosms ensure a necessary degree of realism in the measured processes (Clobert et al., 2018). This setup therefore allowed for a direct test of the hypothesis that basalt application leads to carbonate formation and long-term carbon storage.

2 Material and Methods

2.1 Ecotron facility

At the UHasselt ecotron, large (4.7m^3, diameter 2 m) and deep (1.5 m) macrocosms are exposed to tightly controlled environmental treatments in gas-tight enclosures. High-frequency measurements allow accurate estimation of the ecosystem C budget on an hourly scale (Rineau et al., 2019). In short, the macrocosms were placed within a large, gas-tight chamber topped with a dome transparent to both UV and photosynthetically active radiation (PAR). Within the chamber, environmental conditions including air temperature, precipitation, relative humidity, CO_2 concentration, and wind speed were precisely controlled. Soil temperature and water tension were also regulated using a heat exchange system and a network of suction cups installed at the base of each lysimeter—the vessel containing the soil and plant macrocosm. Each lysimeter was equipped with sensors located at five soil depths (10, 20, 35, 60, and 140 cm) across three radial profiles (spaced 120° apart). These sensors continuously monitored soil temperature, water tension, volumetric water content, and electrical conductivity. Above the plant canopy, air samples were collected to monitor CO_2, CH_4, and N_2O concentrations using two gas analysis systems (LGR 911-0011 and SYNSPEC gas analyser; Envicontrol, Gembloux, Belgium). CO_2 concentrations in each chamber were maintained to mimic future levels (ambient + 221 ppm offset) by automated CO_2 gas injection or scrubbing by extracting air from the chamber and passing it through a lime-filled container. The CO_2 levels were measured every 30 minutes by the means of an air sampler located 1m above the macrocosm's soil surface. The air sample is then conducted to a Synspec gas analyser where its CO_2 concentration is measured using gas chromatography. Additionally, net radiation (incoming minus outgoing radiation) was measured using pyranometers, and PAR was monitored with a LI-190R quantum sensor. All measurements were recorded at intervals ranging from once every 30 minutes to once per minute, depending on the parameter.

Soil water samples were collected *via* suction cups installed at 10, 20, 35, 60 and 140 cm depth and in triplicate in each lysimeter. The tension in the suction cups was adjusted by a vacuum pump (VS Pro, METER group, USA) applying a constant -50 hPa and -150 hPa to the upper (10, 20, 35 cm) and lower (60, 140 cm) cups, respectively, as upper soil layers are usually drier. The water extracted from the cups was then stored in 1L-bottles sitting in a temperature-controlled cabinet (+10 °C). Every three weeks, the water contained in the bottles was filtered at 0.45µm and analysed for total organic Carbon (TOC),

105 total Nitrogen (TN), anions and cations. Four water samples taken from the main pipe feeding the rain system were also filtered and analysed in the same way, as well as water samples from the leachate tank (aliquot of the drainage).

The ecotron served as a real-time, accurate simulator of climate scenarios, controlling air temperature, humidity, rainfall, CO_2 concentration, wind speed, soil temperature, and bottom soil water tension for each macrocosm. High-frequency monitoring was performed for key parameters, including photosynthetically active radiation (PAR), net radiation, lysimeter weight,
110 leachate weight, and concentrations of CH_4 and N_2O. Soil water samples were collected at five separate depths and in triplicate for chemical analysis. More details about the ecotron technicalities can be found in (Rineau et al., 2019; Roy et al., 2021).

2.2 Macrocosms

Six large plant-soil cores were extracted undisturbed from a dry heathland in 'Hoge Kempen' National Park, Belgium, in November 2016 and placed in ecotron units at UHasselt. The soil in this plot is a brunic-dystric arenosol, with an organic layer
115 of 10-20 cm depth, on top of a sandy matrix containing 5-10cm clay lenses, and with a ferric iron precipitation horizon at, 150-200 cm depth. The soil pH varies from 6 on the top, organic layer and 4 to 5 on the B horizon. The TOC content of the soil varies between 1.9% in the top, organic layer and 0.5 % below down to 140 cm. Based on the DOV database (https://www.dov.vlaanderen.be/), the CEC (Cation Exchange Capacity) of this type of soil (classified as Zbf1t) is expected to range between 3 and 8 cmol(+)/kg.

120 We refer to these plant-soil cores as "macrocosms" further in the article. The macrocosms were exposed to recreated ambient climate conditions until January 2020, after which they were "marginalized" by removing topsoil (top 20cm) and vegetation to simulate nutrient-poor marginal land. From January 2020 to September 2022, the macrocosms were subjected to a future climate scenario (2070-2075) and agricultural treatments (NPK fertilization at the same level in all units and Si foliar spraying in three of them) to mimic the conversion of heathland to crop fields. Barley was cultivated with foliar Si amendments, after
125 all units were amended with 10 t/ha equivalent of $CaCO_3$ to raise soil pH (Rineau et al., 2024). This liming increased the pH to 7, which we estimate increased CEC by 1.5-2.5 cmol(+)/kg, resulting in a soil CEC estimated at 4.5-10.5 cmol(+)/kg and largely dominated by Ca^{2+} ions before the basalt application. This was followed by mustard as a cover crop, and mineral NPK fertilization was applied (100 N 80P 120K, with NH_4NO_3, $NH_4H_2PO_4$ and KNO_3). Basalt was added to three units (10 t/ha)

and incorporated into the top 20cm of soil, with all units tilled during seeding. The basalt was fine grade (less than 50µm particle size, with 70-80% of the particles under 20µm, according to manufacturer data) and consisted mostly of plagioclases and pyroxenes (38 and 26%, respectively; for more details see Table S1). The basalt composition was moderately reactive for enhanced weathering, with relatively low olivine (7%) and moderate feldspar (10%) contents, and a maximum potential C removal capacity of 529 kg CO_2/t (144 kgC/t). We applied 10 t/Ha, which theoretically led to a maximum of 1444 kgC/Ha (144.4 gC/m^2) of removal according to the Renforth formula (Gunning et al., 2010; Renforth, 2019) (Table S1). The soil pH at that moment was 7 in all units. Oats were then planted and harvested after 150 days. Manual weeding was carried out during the growing season. More details and a schematic overview are provided in the "macrocosms details" box in the supplementary information.

2.3 Climate simulations

The experiment was conducted under climate conditions projected for 2070-2075 (RCP 8.5 scenario), allowing for realistic simulations of elevated atmospheric CO_2 levels and their effects on the ecosystem (Vanderkelen et al., 2019). Climate data were downscaled to a half-hourly resolution using projections based on local climate models (more details in (Vanderkelen et al., 2019)), and CO_2 levels were adjusted to reflect future increases by adding a 221ppm offset to real-time measurements from a nearby ICOS station. The characteristics of the climatic conditions applied to the six macrocosms are shown in Figure S1.

2.4 Plant biomass C pool

The quantification of plant biomass was conducted to assess the influence of basalt amendment on vegetation development as well as to estimate the overall carbon balance within the ecosystem. At harvest, plant density was measured using three 50 x 50 cm quadrats per macrocosm. In each quadrat, oat stems were counted, and five plants (shoot and root) were randomly sampled for biomass. Plants were dried at 60°C, and dry weights of grains, chaff, stems, leaves, and roots were measured, along with the number of grains and leaves. Yield was calculated based on plant density and grain weight per unit area. Carbon content in oat biomass was estimated by multiplying the dry weight of plant organs by stem density, assuming a 40% carbon content (Sun et al., 2019). For weeds (primarily *Rumex acetosella*), biomass was measured after manual removal, corrected for water content, and scaled to the lysimeter area, also assuming a 40% carbon content. Note that we tested the sensitivity of

our results to this C content assumptions, see the statistics section below. Since the soil was bare at the onset of the experiment during basalt application, the total plant biomass at the conclusion of the study represents the net change in the vegetation carbon pool, and was noted Δ plant C. This value was used to estimate the net carbon flux to the soil (section 2.10).

2.5 CO_2-C net flux

Silicate rock amendments are of interest due to their potential to increase ecosystem carbon (C) sequestration. To verify this, we estimated C sequestration in both plant biomass and soil by measuring net CO_2-C and CH_4-C fluxes. Net CO_2-C flux, the largest component, was calculated as the exchange between the atmospheric compartment and each macrocosm. Given the airtight nature of the chambers and the established relationship between CO_2 changes and injection or scrubbing time, we estimated the net CO_2-C stored or released over time. Fluxes were calculated every 30 minutes and converted to daily rates (g CO_2-C/m²) using the ideal gas law (air temperature on top of the macrocosm as well as air pressure are measured automatically). Data gaps were filled using a moving average function on the linearly interpolated data (ALMA function from the TTR package in R). Interventions in the chambers can slightly disturb the system's carbon balance, as CO_2 levels in the chamber equilibrate with those of the main corridor. During long interventions, CO_2 concentrations inside the chambers were observed to increase from ~400 to ~800 ppm. For a conservative estimate of potential bias, we assumed that the entire excess of 400 ppm was not removed by the ecotron control system but instead fully assimilated through photosynthesis, although this scenario is unlikely. Based on chamber volume, average temperature, and pressure, this would correspond to ~50 mg C fixed per intervention. Scaled to the total number of interventions, this results in an estimated maximum error of ~1 g C in sequestration.

2.6 CH_4-C net flux

The net CH_4-C flux was determined as the exchange of CH_4-C between the atmospheric compartment and the macrocosm. CH_4 concentrations in the growth chambers were measured every 30 minutes using a Los Gatos Research (LGR) gas analyzer. Previous measurements confirmed that methane concentrations remained stable in the absence of a macrocosm and were unaffected by CO_2 scrubbing, but fluctuated rapidly when the chamber doors were opened. These events were therefore identified and corrected for in the flux calculations. Additional tests verified that CH_4 fluxes were not influenced by microbial activity in the drainage system. The CH_4 budget was computed by correcting the CH_4 concentration changes for door-opening

artefacts, then converting the resulting values from ppm to g CH_4-C m^{-2} day^{-1} using the ideal gas law, methane's carbon fraction (75%), and recorded chamber temperature and pressure.

2.7 Rainwater C flux

The amount of carbon (C) added to each macrocosm through simulated rainfall was estimated by multiplying the average non-purgeable organic carbon (TOC measured in a TOC/TN analyser (Leco TCH 600, Leco AG, Mönchengladbach, Germany), after purging carbonates by acidification) concentration in the irrigation water—based on triweekly measurements—with the cumulative precipitation over each corresponding three-week period. Due to the consumption of the total sample volume for TOC and TN analyses, direct quantification of dissolved inorganic carbon (DIC) inputs from precipitation was not possible. Consequently, the atmospheric DIC flux was omitted from the carbon budget. This omission is unlikely to confound the results, as all experimental units were subjected to identical climate projections and rainfall volumes. Furthermore, given the low precipitation volume and the characteristically low carbon concentration of local rainwater, this flux is considered negligible (see Results). Precipitation amounts were estimated using the AWAT model (Hannes et al., 2015; Peters et al., 2017), following the approach described in (Rineau et al., 2024). These values were then aggregated for each macrocosm by summing the contributions over the entire growing season.

2.8 Leachate C flux

We estimated the amount of C leaching out of the macrocosm using the calculation presented in equation 1:

$$1)\ leachateC\ (gC) = leachate(l) \times soil\ waterC(gC/l)$$

"Leachate" refers to the cumulative volume of water collected in each unit's weighable leachate tank during the three-week intervals between sampling events, while "soil water C" denotes the average non-purgeable organic carbon concentration in the soil water samples collected at each sampling date. Based on prior experience, the values exceeding 50 mg/L were considered outliers and excluded from the calculations. Final values were aggregated by summing the carbon fluxes per unit over the entire growing season.

2.9 Sampling C flux

Some of the macrocosm C has also been exported through soil water sampling throughout the experiment. To account for this, we used the calculation presented in equation 2:

$$2)\ samplingC\ (gC) = 10\ (l) \times\ 12\ \times\ average\ C\ (gC/l)$$

Where 10 corresponds to the average amount of water collected per unit per sampling campaign (10 l in every unit); 12 is the number of sampling campaigns during the experiment; and "average C" is the average non-purgeable concentration in this unit throughout all samplings. The obtained values are therefore a C flux aggregated through the whole growing season.

2.10 Soil C net flux

In the previous sections, we described the measurements of the following fluxes: CO_2-C net flux, CH_4-C net flux, rainwater-C flux, leachate C flux, sampling C flux, as well as the difference in plant C pool size. The only unknown flux needed to close up the C budget of the ecosystem is then soil C net flux, that was calculated as a difference between the abovementioned integrated fluxes (gas-, leachate-, sampling) and the difference of plant C pool size. Indeed, under the closed conditions of the macrocosm, any carbon not sequestered in plant tissue is assumed to have been partitioned into the soil matrix. :

$$3)\ soilC = \sum\ \ (CO2C + CH4C + rainfallC - leachateC - samplingC) - \Delta\ plantC$$

Where "soilC" is the soil C net flux; "CO2C" is the CO_2-C net flux (negative if the macrocosm was a net sink of CO_2-C); CH4C is the CH_4-C net flux (negative if the macrocosm was a net sink of CH_4-C); rainfallC the rainwater-C flux; Δ plantC is plant biomass C pool (positive), leachateC the leachate C flux and samplingC the sampling C flux; all fluxes are expressed in grams of C. Since plant biomass was measured only once, at harvest, carbon budget could only be closed over the entire growing season. Consequently, all related data were aggregated across the full experimental period (01/03/2022–01/09/2022). The net CO_2-C flux inherently accounts for both photosynthetic uptake and respiratory losses, and we were not able to differentiate between the two.

s2.11 Soil C pools

To assess if EW resulted in the formation of inorganic C, we estimated the size of the different organic and inorganic C pools (dissolved organic C: DOC, dissolved inorganic C: DIC, soil organic C: SOC and particulate inorganic C: PIC). We monitored

DIC by measuring the sum of carbonates, bicarbonates, and carbonic acid and DOC by measuring non-purgeable organic C in soil pore water collected from five depths (10, 20, 35, 60, and 140 cm) at three-week intervals throughout the experiment. We measured concentration of Soil Organic Carbon and Soil Inorganic Carbon at the end of the experiment and then assessed the difference between control and basalt-treated macrocosms to determine whether there has been an effect of the treatment on the formation and storage of PIC and SOC. PIC was measured to account for possible precipitation of carbonate ions. At the end of the experiment, we collected 3 randomly taken soil samples per unit and dried them overnight in an oven at 60°C. Then, PIC was measured as total inorganic carbon (carbonates) in soil sample after drying, and was measured by measuring CO_2 formation after acidifying soil sample with phosphoric acid in TOC/TN analyser (Leco TCH 600, Leco AG, Mönchengladbach, Germany). Finally, SOC was measured as total organic carbon on a TOC/TN analyser (Leco TCH 600, Leco AG, Mönchengladbach, Germany) on dried soil samples.

2.12 C isotope analyses

We aimed to rule out the possibility that the basalt directly reacted with CO_2 from the atmospheric pool rather than with CO_2 derived from soil respiration. This process can be effectively traced using isotopic analysis, as the CO_2 supplied by the ecotron's control system has a distinctly negative $\delta^{13}C$ signature. If atmospheric CO_2 were directly fixed by the basalt, it would result in a detectable shift toward more negative $\delta^{13}C$ values in the soil carbon pool. With strong isotopically fractionating C-assimilation linked to photosynthesis, it is possible to trace and differentiate the plant-derived C, serving as a substrate to the soil organic carbon (SOC, $\delta^{13}C$ = - 27.0 ‰ vs. VPDB, see Figure S2) and being respired from CO_2-C, which might be directly adsorbed from the isotopically enriched signal being supplied into the ecotron via CO_2 tanks (-30 ‰ vs. VPDB). Thus, if the treatment with basalt would result in a shift of the isotopic ratio of the soil carbontowards the atmospheric value, this would be indicative of adsorption with further incorporation from this source into the soil carbon.

Soil samples were taken in September 2022, at the end of the experiment. They were dried (60°C, 24 h, atmospheric pressure) and subsequently milled using a ball mill (MM2, Retsch, Haan, Germany). Samples were then weighed into tin foil and measured against a lab standard (acetanilid, p.a., IVA Analysentechnik, Meerbusch, Germany) calibrated against international standards (IAEA CH-7 and IAEA CH-3, International Atomic Energy Agency, IAEA, Vienna, Austria) using an Elemental analyser (EA IsoLink CN, Thermo Fisher Scientific, Germany) connected via a continuous flow open split interface (ConFlo

IV, Thermo Fisher Scientific, Bremen, Germany) to an isotope ratio mass spectrometer (DELTA V Advantage, Thermo Fisher Scientific, Bremen, Germany). All $^{13}C/^{12}C$ ratios are reported using the δ-notation against the internationally recognized ratio of Vienna Pee-Dee Belemnite (VPDB) and expressed in per mille (‰) (Coplen, 2011; McKinney et al., 1950) in equation 4:

$$4)\ \delta^{13}C = (R_{sample}/R_{standard} - 1)$$

where R represents the ratio of the heavier to the most abundant stable isotope of the corresponding element (e.g., $R = {}^{13}C/{}^{12}C$), with $^{13}R_{VPDB} = 0.0111802$, as recorded in the software (Isodat 3, version 3.0.94.12, Thermo Fisher Scientific, Bremen, Germany).

2.13 Effect of treatment on soil CO_2 adsorption capacity

Finally, we investigated whether the observed increase in soil carbon in the basalt-amended macrocosms could be attributed to a purely physical adsorption mechanism. Silicate rock powders possess a high surface area and a crystalline structure capable of adsorbing various gases (Ramos et al., 2022), and could, in principle, retain CO_2 from soil respiration in the gaseous phase. To test this, we conducted a series of experiments on soil samples from the macrocosms to evaluate their CO_2 adsorption properties. We investigated whether the observed increase in soil carbon in the basalt-amended macrocosms could be attributed to a purely physical adsorption mechanism. We validated this assumption by conducting additional continuous-flow CO_2 adsorption experiments using a humid CO_2/Ar gas mixture (RH = 100%, CO_2 concentration = 28.5 vol%).

2.14 Soil Ca and Mg concentrations as proxy for weathering

Cation weathering products (Ca2+, Mg2+) were measured to provide a mass-balance estimate of carbon sequestration. This approach compensates for potential CO2 losses via degassing during storage by focusing on the stable mineral-derived cations that drive the sequestration reaction. In the same soil pore water samples as described in 2.11 (hence at 10, 20, 35, 60 and 150cm), the concentration of Mg^{2+} and Ca^{2+} in soil solution was determined using inductively coupled plasma–optical emission spectrometry (ICP-MS, Analytik Jena 820MS).

2.15 Microbial metabolic activity

Microbial metabolic activity in soil was measured to compare basalt and control treatments and to help interpret soil C fluxes. The FDA (Fluorescein Diacetate) assay, which estimates microbial activity by measuring the conversion of fluorescein

diacetate to fluorescein by microbial enzymes, was used (Adam and Duncan 2001). For 13 consecutive days in May 2022, three soil samples (1 cm diameter, 10 cm deep) were collected per macrocosm, stored at -19°C, sieved, and aliquoted to 0.1 grams dry weight. Samples were incubated in sodium phosphate buffer with FDA solution at 30°C for 16 hours. After dilution, absorbance was measured at 490 nm, and values were converted to moles of substrate using a calibration curve.

2.15 Statistics

Data in Figure 1 summarize total carbon fluxes during the growing season, corresponding to single-time-point biomass measurements taken at harvest. However, hourly CO_2-C net flux recordings enabled finer-scale analysis, so we evaluated treatment impacts on daily CO_2-C net flux using a linear mixed-effects model incorporating treatment, ecotron unit, and day as factors. Each flux is associated with its own standard deviation. Two components, "plantC" and "leachateC" were estimated through an internal bootstrap procedure to account for uncertainty arising from stem density estimates, the C content of plant organs (20% to 60%)(plantC) and the amount of water sampled per sampling event (5 to 15l). To propagate uncertainty across the entire soil C net flux calculation, we used a bootstrapping approach (n = 10,000) to generate empirical distributions of the soil C net flux for each treatment. We then applied a bootstrap hypothesis test to evaluate the observed treatment effect against a null distribution assuming no treatment difference. Additional analyzes employed similar modeling approaches for other variables including organ-specific biomass, stem density, soil C isotopes, and inorganic C in soil water. For inorganic C in the soil solution (DIC), as well as Ca and Mg in the soil solution, as the dataset was sparse, but also more structured from the fixed variables depth and date, we used a different bootstrapping approach. We generated empirical distributions of the concentration of the element (iC, Ca or Mg) in soil solution at the unit level (in order to keep the structure induced by depth and date). We then ran a generalized linear model with treatment, depth and their interaction as fixed variables and unit and date as random variables, and computed the average estimate and p-value of the effect of treatment across all iterations (n = 1,000). Statistics were done in R (R core team, 2019) using nlme (Pinheiro et al., 2023), dplyr (Wickham et al., 2023), lubridate (Grolemund & Wickham, 2011) and vegan (Oksanen et al., 2013) packages.

3 Results

3.1 Climatic conditions

The spring began unusually cold with night frosts and temperatures below 5°C in early March, rapidly transitioning to warmth in April (20°C maxima) and subsequent heatwaves in May (30°C). Summer remained consistently warm, punctuated by a late-June heatwave. Rainfall was frequent yet light (<15mm/day) throughout most of the growing season except for brief periods of drought and heavy rains in mid-May and early June. Consequently, soil moisture fluctuated between extremes: rapid depletion to ~5% during the May heatwave, short-lived recoveries exceeding 10%, and sustained lows (<5%) throughout summer (Figure S1).

3.2 Effect of basalt amendment on ecosystem C fluxes

The largest input flux, by far, came from net CO_2 exchange (366 to 457 gC/m^2 in control and basalt treatments, respectively), which was almost two orders of magnitude larger than all other fluxes (1 to 7 gC/m^2 depending on the flux and the treatment) (Figure 1). The crop system was a net CH_4 sink throughout the experiment, but the treatment had no effect on methane balance of the macrocosm. The macrocosm was a net C sink in both treatments (456 gC/m^2 and 361 gC/m^2 in basalt and control units, respectively).

310

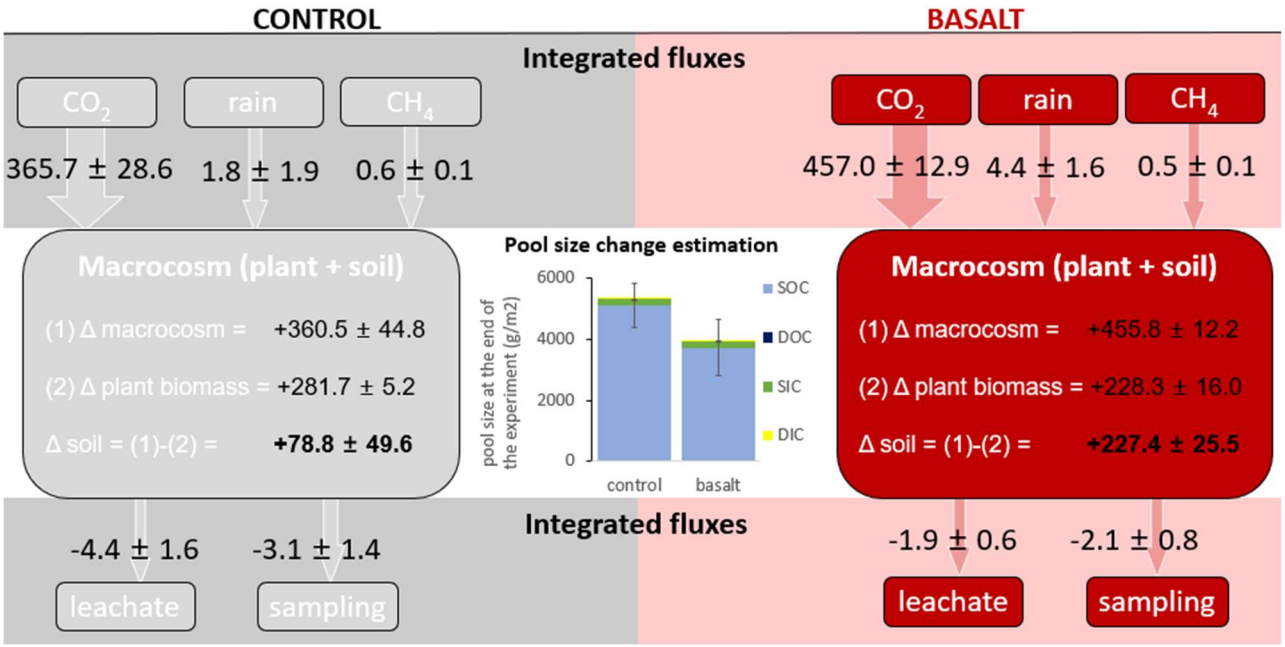

Figure 1. Measured net C fluxes and pools to the macrocosms in both treatments (black: control, red: basalt), in g/m² aggregated for the whole growing season (01/03 to 01/09: 185 days), and averaged per treatment (n=3; +/- standard error). Integrated fluxes are displayed in italics; measurements of pool sizes are given in the "macrocosm" boxes. The total macrocosm C pools entailed plant and soil C pools, plant C pool being measured as the plant biomass at the end of the experiment and soil C pool calculated as a difference between total macrocosm C pool and the plant pool. Negative values indicate a net loss of C from the soil, and positive values indicate net Csoil accrual. Note that the sampling pool corresponds to the soil pore water sampling occurring every 3 weeks. The absolute size of every soil C pool (g/m2) as measured at the end of the experiment is displayed in the center of the figure as a stacked barplot (bars=standard deviation).

We then partitioned the sequestered carbon (C) within each macrocosm into two primary pools: plant biomass and soil. Plant biomass was significantly lower in the EW treatment (228 g C/m² vs. 282 g C/m² in the control) (Figure S3). Notably, the estimated root biomass was relatively low, comprising only 6% of total plant dry mass (Figure S4), whereas values reported in the literature typically range between 15% and 30% for oat (Gao et al., 2019). Despite thorough sampling, it is possible that some root biomass remained in the soil, potentially leading to an underestimation. Based on this discrepancy, we estimated that root biomass may have been underestimated by 10–59 g C/m²; note that this affected the two treatments equally

Approximately 40% of the total fixed C was allocated to the soil pool (153 ± 41 g C/m² across treatments) (Figure 1). The basalt treatment led to a substantial and statistically significant increase in soil C sequestration, with values 2.9 times higher

(227 ± 26 g C/m²) than in the control (79 ± 50 g C/m²), corresponding to a difference of 149 g C/m² (p = 0, bootstrap test; note that the bootstrapped difference in mean values was 155 g C/m², see Figure S5). These results were robust to assumptions in pore water sampling flux (5 to 15 L per sampling date; p = 0 and 149 to 150 g C/m² in soil sequestration) and plant C content (20% to 60%; p = 0 and 133 to 197 g C/m² in soil C sequestration). A peak of CO_2 emissions occurred immediately after soil disturbance (tillage for seeding), and this peak was larger under basalt treatment (Figure 2). Subsequently, both treatments exhibited comparable CO_2 dynamics until mid-May/mid-June when differences emerged, accelerating sharply during the June/July heatwave before stabilizing later in the season (Figure 2). These trends coincided with rising soil temperatures (~20°C). Despite lacking separation of plant vs. soil-derived carbon, negligible variations in final biomass suggest the observed

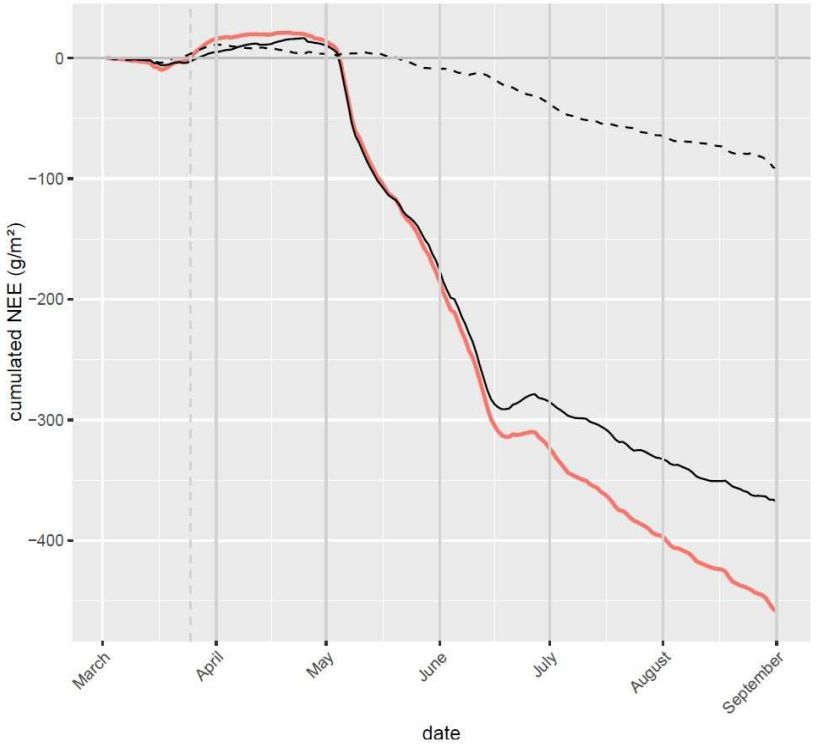

patterns reflect differential soil carbon sequestration. Notably, changes in net carbon balance were strongly inversely linked to soil temperature (Figure S6) rather than moisture.

Figure 2. Effect of the EW treatment on the dynamics of the C balance of the system. Black: control, Red: basalt treatment; dashed black line: difference between the two treatments; vertical dashed grey line: date of the basalt amendment. The NEE (Net Ecosystem Exchange) has been estimated per hour and per unit (three units per treatment) using a model accounting for CO2 corrections, temperature and pressure, and aggregated per day (sum) and then per treatment (average) and cumulated throughout the growing season. We also computed the difference between the average in the two treatments (dashed line). Standard error is added to the figure as black (control) and red (basalt) shaded areas but are barely visible because of their low values.

3.3 Soil carbon

No significant differences in concentrations of dissolved inorganic carbon in soil pore water were observed between treatments at any depth (Figure S8), even when using bootstrap approach to address the sparse nature of the dataset (difference between estimate of treatment "control" and "basalt" after bootstrapping= -0.72 +/- 1.49, average p-value=0.43) with both inorganic and organic C levels remaining below 0.2 gC/m² (1–5 mgC/L) (Table 1). To adjust for varying relevance of dissolved inorganic carbon increases across depths, we normalized values according to the respective soil column volumes and moisture contents. Specifically, an increment of 10 mg/L in shallow layers (short columns, lower moisture) contributed less significantly to the overall budget compared to deeper strata (longer columns, higher moisture). After multiplying inorganic C values by adjusted soil volumes and moisture, bootstrapping yielded statistically nonsignificant results.(difference between estimate of treatment "control" and "basalt" after bootstrapping= 9.7 +/- 16.5 mgC/l, average p-value=0.43). Additionally, we re-ran the bootstrap analysis focusing exclusively on post–May 17th data, given the emergence of significant basalt-treatment effects on Net Ecosystem Exchange (NEE) thereafter. Nevertheless, this refined analysis still failed to reveal any discernible differences in dissolved inorganic carbon among treatments (estimate of treatment "control"= 21.2 +/- 23.3, average p-value=0.55). No significant treatment-related changes in calcium or magnesium concentrations were detected in soil pore waters (for Ca: difference between estimate of treatment "control" and "basalt" after bootstrapping= -3.17 +/- 3.28, average p-value=0.28; for Mg: 0.14 +/- 1.76, average p-value=0.59, Figure S7). The soil pore water samples were subjected to at least two manipulations during which they were exposed to a low CO_2 partial pressure in the headspace: first, during storage in the collection bottles for up to three weeks, and second, during filtration and aliquoting into 20 mL vials. Under these conditions, dissolved carbonates may have partially degassed as CO_2. The results presented in Table 2 show the size of the C pools at the end of the experiment. Values of PIC showed no significant differences between treatments (222 ± 13 g/m² in the basalt-amended plots vs. 214 ± 3 g/m² in controls; t-test, p = 0.28) (Table 2, Figure S8). Because pool sizes were not measured at the beginning of the experiment, it is possible that control plots already contained higher C pools initially. We did not observe statistically significant differences in SOC pool size between the treatments (Figure S9). Although mean values appear higher in the controls, the variability is considerable, as indicated by the large standard errors. The relative size and variability of these pools (3713 ± 320 g/m² in the basalt treatment and 5086 ± 921 g/m² in the control; see Table 2) compared to the measured fluxes, means that increase in pool size due to the measured C sequestration fell within the range of measurement uncertainty.

Table 1. Inorganic carbon concentration of soil water samples taken by suction cups. The suction cups were installed at 5 different depths, and set at a tension of -150 HPa until 35cm deep and -50 HPa below. Soil water was sampled every 3 weeks and analysed for TOC and inorganic C. Grey: values above 5 mg.l^{-1}.

unit	depth (cm)	15/03	5/04	26/04	17/05	7/06	28/06	19/07	9/08	30/08
1	10		15,6	8,8		3,8	11,2	11,5		
	20		4,8	4,9	4,4	4,5				
	35		1,6	1,6	1,5	1,2	4,3	1,5		4,5
	60		1,3	4,5	0,7	0,6	4,3			
	140						14,8			
3	10		3,2	7,8					5,0	
	20							3,8	4,0	
	35		1,5	1,5	0,7	4,5				4,4
	60		0,9	1,2	0,7	1,3	1,0			
	140	1,1		0,9	0,8	0,8	0,9			
4	10			4,3	3,9	1,0	3,0			
	20		4,5	4,3	3,5	1,7		4,0		4,0
	35		4,5	3,4	1,4	5,3				
	60									
	140								7,2	
Basalt		1,1	4,2	3,9	2,0	2,5	5,6	5,2	5,4	4,3
6	10					1,9				
	20					6,2				
	35		4,7	0,8	3,6			3,6	4,9	4,3
	60	0,9	0,9	0,8	0,7	0,9	0,6			
	140	0,9	0,9	0,8	0,7	0,9	0,8			
10	10				3,9	5,5				
	20		4,8	5,4	3,9		4,1		4,3	4,0
	35	1,2	1,5	1,6	1,2	5,0		3,9	4,2	
	60	1,3	1,5	1,3	0,7	1,4				
	140	1,9	1,9	0,9	1,5	3,3	5,0			
11	10		1,8	4,0	4,1	6,4				
	20		5,1		4,3		4,8			
	35				0,8					
	60		1,0	0,8						
	140									
Control		1,2	2,4	1,8	2,3	3,5	3,1	3,8	4,5	4,2

Table 2. Size of C pools in the topsoil (0 - 20 cm) of the macrocosms, in gC/m^2 measured at the end of the growing season. SIC: Soil Inorganic Carbon, measured as soil dry mass in the topsoil (0-20 cm) samples. SOC: Soil Organic Carbon, measured as mmol/gDW in 20 cm deep soil samples. DIC: Dissolved Inorganic Carbon, measured as total C minus total organic C concentration (mg/l) in 10 and 20 cm soil water samples collected throughout the growing season by the lysimeter suction cups. DOC: Dissolved Organic Carbon, measured as organic C concentration (mg/l) in 10 and 20 cm soil water samples collected throughout the growing season by the lysimeter suction cups. All four parameters were converted to gC m^{-2} in the top 20 cm by accounting for a density of 1.3, 12g/mol C, and 10 % soil moisture for DIC and DOC (average moisture in the top 20 cm of soil across the growing season). Orange cells: concentrations above 5mg/L; red cells: concentrations above 10mg/L.

treatment	Basalt		control	
	average	standard error	average	standard error
SIC	222	13	214	3
SOC	3713	720	5086	921
DIC	0.03	0.03	<0.01	<0.01
DOC	0.13	0.03	0.10	0.06

3.4 Contribution of soil C in the gas phase: CO_2 adsorbed to the basalt powder

Thermogravimetric analysis revealed that the presence of basalt approximately doubled the soil's CO_2 adsorption capacity. However, desorption tests confirmed that the CO_2 was held through weak, reversible physical adsorption, accounting for 0.170 wt% and 0.036 wt% for basalt-amended and control soils, respectively (Table S2). These numbers were negligible in comparison with the other estimated C fluxes.

3.5 Direct fixation of atmospheric CO_2 by basalt

Finally, we aimed to rule out the possibility that the basalt directly reacted with CO_2 from the atmospheric pool rather than with CO_2 derived from soil respiration. This process can be effectively traced using isotopic analysis, as the CO_2 supplied by the ecotron's control system has a distinctly negative $\delta^{13}C$ signature. If atmospheric CO_2 were directly fixed by the basalt, it would result in a detectable shift toward more negative $\delta^{13}C$ values in the soil carbon pool. Although Figure S2 does not allow us to observe temporal shifts in TOC $\delta^{13}C$ (since we did not measure TOC before and after incubation under an isotopically distinct atmosphere), it does allow comparison between treatments. The lack of a meaningful difference in TOC $\delta^{13}C$ between the basalt and control treatments suggests that direct incorporation of atmospheric CO_2 into soil inorganic carbon via basalt was negligible. This result is consistent with expectations, given the position of basalt in the topsoil and the difference between soil and atmospheric CO_2 concentrations.

3.6 Microbial activity

Microbial activity was significantly higher (+32% on average, p=0.005) in basalt-treated soils midway through the growing season (Figure 3).

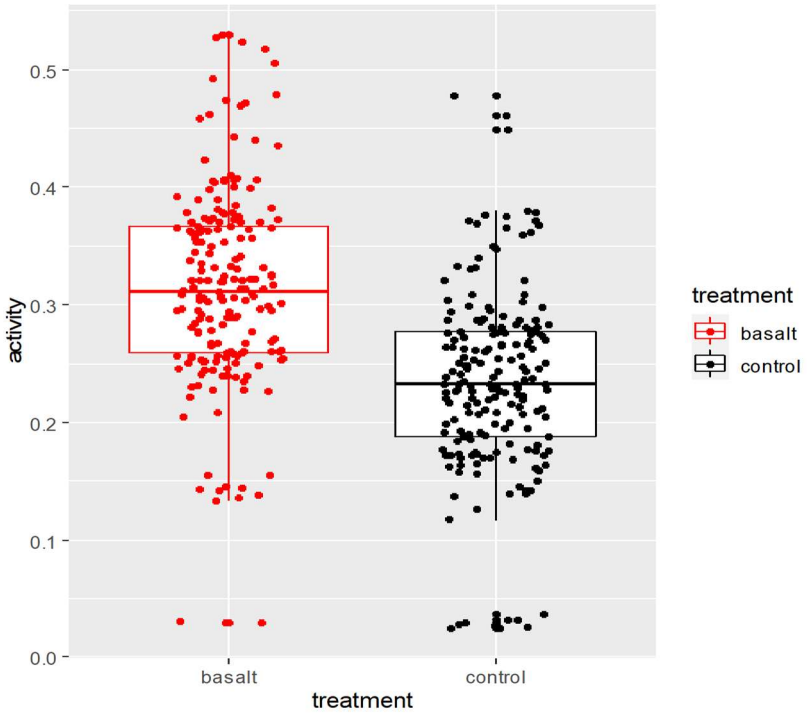

Figure 3. Effect of basalt amendment on microbial activity measured via the Fluorescein Diacetate (FDA) assay during one week at the end of May 2022. The effect of treatment was tested using a mixed model with the metabolic activity as dependant variable and treatment as independent variable, with unit as random variable. Values are expressed in µg of fluorescein released $mL^{-1}.h^{-1}$.

4 Discussion

4.1 EW enhanced fluxes to soil C pools substantially

Our study demonstrated a 2.9-fold increase in net ecosystem exchange under EW treatment, which increased by 150 g/m^2 over one growing season, despite higher initial CO_2 emissions immediately after seeding. Robust sensitivity analyses supported this finding. Because all plots were tilled during seeding and basalt was applied at that stage, there is no clear reason why the basalt-amended plots should have undergone greater disturbance or CO_2 release; we propose instead that the presence of basalt may have stimulated microbial activity, resulting in elevated CO_2 emissions a few days after application in the treated plots. Relative to baseline conditions, and based on the following reasonable assumptions (macrocosm volume of 4.4 m^3, of a mean

bulk density of 1.6 kg/dm³, in a 7 ton dry soil mass, and a mean total organic carbon (TOC) content of 0.7% (1.9% in the top 20 cm, 0.5% below, down to 140 cm depth)) this equated to a 1.2% boost in total soil carbon, far surpassing the "4 per 1000" initiative's goal for mitigating climate change (Minasny et al., 2017). This is especially significant given that our experimental macrocosms were established on marginal soils, where increases in soil organic carbon are typically associated with improvements in soil health, such as reduced erosion, enhanced water retention, and greater nutrient storage capacity. These results confirm that enhanced weathering—a potentially low-cost strategy—could strengthen both carbon sequestration and soil health on marginal lands (Ivan A Janssens et al., 2022), particularly in the Global South. It is important to note that these results were obtained on soil with initially low SOC, as the experimental site was established by converting heathland into cropland through removal of topsoil and vegetation. This initial condition likely influenced the processes observed. In particular, because the soil was far from C saturation, its capacity for additional C sequestration was relatively high. For example, mineral surfaces available for association with newly formed organic matter were more likely to be unoccupied, creating conditions that favored stabilization of fresh C inputs. Thus, the experiment was conducted under circumstances representing a situation with one of the highest potentials for C sequestration.

The amounts of C sequestered in our study correspond to an increase of 0.17 tons of carbon per tonne of basalt amendment applied, falling within the range observed in other EW field trials (Ramos et al., 2022; Swoboda et al., 2022). However, most studies cited in these reviews involved amending with non-basaltic rocks and assessed performance over multi-year timescales. A more analogous study by Kelland et al. (2020) similarly reported equivalent levels of carbon sequestration using basalt, along with a comparable fold-increase versus controls (fourfold instead of threefold here). However, this outcome was achieved under a considerably larger amendment dosage (100 tons per hectare), only inorganic C was considered, not organic C, and the reported sequestration was a modelled value. Alternatively, carbon sequestration rates nearing 2 tons per hectare were realized within a single year using equal amendment quantities (10 tons per hectare), though this involved utilizing a more chemically reactive substance—olivine—as opposed to basalt, and no direct proof of inorganic C sequestration was found, only C removal potential using Mg as a proxy (Dietzen et al., 2018). Thus, the quantity of carbon sequestered in our investigation notably exceeds typical expectations given the amendment type and dosage.

Let us explore potential influences on the observed carbon sequestration rates in our experiment. Firstly, the ambient CO_2 concentration was artificially raised by approximately 200 ppm as part of a broader research program investigating various amendments' responses to projected climatic conditions (Rineau et al., 2024; Schroeder et al., 2021). Enhanced CO_2 levels are known to stimulate both weathering rates and CO_2 uptake via geochemically-driven reactions (Amann et al., 2022). Additionally, elevated atmospheric CO_2 enhances crop biomass production (Kimball, 2016), amplifying carbon inputs into the soil via root exudation. Secondly, we also measured significantly higher microbial activity in basalt-amended soils, mirroring findings by Li et al. (2020), who found a 33% increase in microbial activity following enriched rock-dust applications in orchards. Moreover, (Steinwidder et al., 2025) and (Klemme et al., 2022) reported enhanced degradation of soil organic matter following basalt treatment, which is often accompanied by increased microbial activity. Such higher microbial activity can lead to localized elevations in CO_2 concentrations adjacent to amendment sites. Thirdly, soil structures were preserved in our macrocosms, unlike the column-based study by Kelland et al. (2020), where extensive soil sieving may have disrupted native soil structure, fauna and mycelium networks, thus emphasizing the importance of soil organisms in sequestration processes. Fourthly, however, and most importantly, the degree of carbon sequestration achieved—approximately 17% of the applied basalt amendment within a single growing season—is sevenfold higher than comparable studies using basalt, even though some of them were based on modelled values (Kelland et al., 2020). Remarkably, this figure slightly exceeds the theoretically achievable limit of converting applied basalt into entirely carbonates (144 kg/ha for a 10 t/ha amendment). Hence, either complete transformation of the amendment occurred exceptionally swiftly within three months, which appears improbable based on existing literature (Kelland et al., 2020), or alternative mechanisms contributing to soil carbon sequestration must be considered.

At the conclusion of the experiment, the observed differences in soil organic carbon pools between treatments exceeded the increase in size predicted by our integrated flux budgets (NEE). Because i) the observed NEE reaches the stoichiometric limit of basalt weathering alone—as defined by the Steinour and Renforth formulations— and ii) we did not detect significant increases in the inorganic C pools, we assume that the end destination of this NEE flux must be attributed to organic carbon storage. Yet, the spatial variability of the SOC pool (even within a single lysimeter) is such that this sequestration signal is effectively obscured by biological variation. The difficulty in reconciling these values highlights the 'signal-to-noise' problem

inherent in soil carbon monitoring. Because the magnitude of sequestration over several years is typically small compared to the large and variable background SOC pool, detecting a 1.2% shift is analytically challenging (Bradford et al., 2015). In fact, under the sampling constraints of the current study (one year and limited soil sampling possible), these small-scale accruals would remain statistically indistinguishable from natural soil variability (Smith, 2004). Consequently, integrated flux-based measurements, such as Net Ecosystem Exchange (NEE), emerge as a more sensitive and reliable metric for detecting short-term carbon drawdown (Conant et al., 2011). We therefore proceed with the following discussion by evaluating the observed carbon sequestration through the lens of NEE.

4.2 No evidence for inorganic C formation

This high C sequestration was moreover not followed by noticeable increases in soil inorganic C pools, contrary to expectations with EW. The experimental design did not allow us to take soil samples before the experiment and therefore to understand how different C pools were affected by the treatment, we can only compare the size of the pools in both treatments.

We did not detect any significant increase in soil inorganic C, whether in solution or as particulate inorganic C. We therefore have no evidence of carbonate ion formation, which used to be the central premise of EW. The sequestered carbon was not detected in plant biomass or as gas trapped within amendment pores either. The most surprising result was the lack of dissolved carbonates in soil solutions. Due to gaps in soil-water chemistry data (particularly scarce samples from drier upper layers), a comprehensive carbon budget could not be constructed. Bootstrap analyses indicated no intertreatment disparities in dissolved inorganic carbon, nor any evidence of EW-relevant Ca/Mg ion in soil pore water solution. Nevertheless, four plausible explanations remain for why bicarbonates might have gone undetected: *first*, carbonate genesis occurs at the surface only if precipitation outpaces mass transport. If mass transport is faster than precipitation, carbonate can form deeper rather than being confined to the top 20cm, where we took our samples from; *second*, even small concentration changes over a three-week interval—the frequency of our sampling—could translate into significant cumulative storage at the macrocosm scale over an entire growing season; *third*, the number of samples collected during the driest period was limited, which could also explain why carbonate formation was not captured. However, an increasing number of publications report EW trials where the silicate rock amendments did not lead to any evidence of carbonate formation, whether directly or indirectly through Mg and Ca release in soil solution (Amann et al., 2020; Steinwidder et al., 2025; Vienne et al., 2024); *fourth*, the Ca and Mg freed by the

EW reaction could have been immediately taken up by the plants or adsorbed to soil colloids. Therefore, although our data provide no direct evidence for EW-mediated reactions, methodological limitations prevent us from drawing definitive conclusions regarding their occurrence. At the same time, we cannot exclude the possibility that some carbon was sequestered through pathways other than carbonate formation.

4.3 Extra mechanisms of C sequestration

This methodologic bias fails anyway to adequately explain the observed extent of soil carbon sequestration. Complete dissolution of the amendment through EW within such a brief timeframe is implausible and insufficient to account for the entirety of sequestration. Temporal dynamics of sequestration merit particular scrutiny: initiation coincided with topsoil temperatures crossing a 20°C threshold, occurring comparatively late in the growing season when significant plant biomass had already developed. Intensification during a concurrent heatwave underscores thermal dependency. Limited soil moisture throughout the season reduced moisture-related constraints on EW reactions (Guo et al., 2023). Isotope evidence also showed that the EW treatment did not directly interact with the atmospheric C pool instead of the CO_2 coming from soil respiration.

The observed increase in soil C sequestration could be linked to enhanced CO_2 uptake by plants. The amendment may have stimulated photosynthetic activity, thereby increasing belowground carbon allocation via root exudates. We speculate that under the amendment, root exudates interact with fine particles of the silicate rock, creating organo-mineral complexes that are making C recalcitrant. Indeed, weathering products of basalt are known to undergo such reaction, and these results could partially illustrate the synergy between EW and SOM accrual described by (Buss et al., 2024), despite the absence of clear evidence of EW in our study. Indeed it has been shown that mineral-associated organic matter (MAOM) is a strong stabilizing factor for organic matter (Cotrufo et al., 2012). However MAOM formation cannot account for all of the sequestration observed, as it is dependent of formation of secondary minerals from EW, especially since basalt is known to be more reactive for EW than for SOM accrual (Buss et al., 2024). In fact, the effects of EW on MAOM are still unclear, as several studies found either an increase (Sohng et al., 2025), either a decrease (Sokol et al., 2024) in MAOM pool size after silicate rock amendments.

Alternatively, basalt may stimulate root exudation, facilitating interactions with pre-existing soil constituents to produce particulate organic carbon (POM) or additional MAOM. However, root exudates constitute merely 5–10% of assimilated

carbon (yielding a maximum contribution of 0.1–0.2 t/ha), which would contribute to only a fraction of the excess sequestration. However, formation of aggregates due to abiotic process of Ca and Mg provided by the basalt also played a significant role in the sequestration potential, as was observed before by (Buss et al., 2024), especially since the basalt used in our study was 3 times richer in these elements than in that publication. However, according to the same study, plant should reduce this protection through plant exudates solubilising Ca and Mg (Buss et al., 2023). Root biomass was very low, suggesting that plant reduction of soil aggregation was limited. However, we did not observe clear solubilization of Ca and Mg; but we cannot rule out this process for the same reason of low sampling intensity from end of May onwards. It is therefore possible that organic matter decomposition products may play a role as well there, and that labile organic C initially present in the soil and/or resulting from the decomposition substantially contributes to this very high sequestration rate.

While we observed no significant change in total plant biomass, the increased NEE in the basalt treatment suggests a strategic shift in carbon allocation toward below-ground fluxes. Although root exudates alone are unlikely to fully account for the total magnitude of carbon storage observed, we speculate that they could have served as a primary substrate for the enhanced microbial activity (FDA) measured during the growing season. This stimulation may have been responsible for the initially higher soil CO_2 emissions; however, if the Microbial Carbon Use Efficiency (CUE) is higher under basalt treatment, this metabolic throughput leads to a net accrual of microbial necromass that exceeds respiratory losses. Under this 'microbial carbon pump' hypothesis, the improvements in soil biochemical conditions and the abundance of fresh mineral surfaces provided by the basalt facilitate the rapid transfer of metabolized carbon into stable associations with soil minerals. Such 'microbial entombment' produces highly recalcitrant carbon forms (Xiao et al., 2023) and is consistent with our observation of increased enzymatic potential alongside a net carbon sink. If microbial turnover is particularly rapid, this pathway could explain the significant organic carbon sequestration measured in our experiment even in the absence of standing biomass gains or inorganic carbonate accumulation. This suggests that microbial entombment may represent a carbon storage pathway for enhanced rock weathering that is comparable in importance (and perhaps more immediate in detection) to carbonate formation.

5 Conclusion

Our results demonstrate that basalt application significantly enhances the capacity of crop ecosystems to act as carbon sinks, tripling soil carbon sequestration over a single growing season. Basalt treatment shifted the macrocosms from marginal (0.5 tC/ha) to substantial (1.5 tC/ha) carbon sinks, successfully overcoming the initial carbon losses associated with soil disturbance during application. While we found no direct evidence of inorganic carbon sequestration via carbonate formation, potentially due to an incomplete dissolved inorganic carbon (DIC) budget, the total carbon accrued exceeded what could be attributed to weathering alone. These findings suggest that the indirect effects of weathering, such as the stimulation of mineral-associated and particulate organic matter, could be the primary drivers of carbon storage in this system.

Author contribution

FR, MM, VP, PS, WS, BS, RZ and EL contributed to conceptualization, methodology and validation. FR, AHF, JG, KG, AL, DK, MMD, BP, JP, TP, TR, XS, HV, JV, and MZ contributed to analysis and data curation. FR wrote the original draft. FR, AHF, JG, AL, DK, MM, VP, PS, WS, BR, HV, JV, RZ and EL reviewed and edited the draft. FR, AHF, JG, AL, DK, TP, HV, JV contributed to the figures. FR, MM, VP, PS, WS, BR, RZ and EL contributed to the funding acquisition.

Competing interests

The authors declare that they have no conflict of interest.

Acknowledgements

We thank Carina Bauer and Petra Eckert of the Centre of Stable Isotope Research in Ecology and Biogeochemistry (BayCenSI, www.censi.uni-bayreuth.de) for their skilful technical assistance, and we thank Maria Sharro for assistance with graphical design of figures used in the manuscript. The authors used artificial intelligence tools (ChatGPT) to assist with English language editing of the manuscript.

Financial support

The study was supported by the FACCE-SURPLUS project BiofoodonMars, and financed by the Flemish Fonds voor Wetenschappelijk Onderzoek (FWO). D.I.K. and J.V.V. acknowledge the support by the Ministry of Science and Higher Education of the Russian Federation for Boreskov Institute of Catalysis (project no. FWUR-2024-0032 and FWUR-2024-0036)

References

Amann T, Hartmann J, Hellmann R, Pedrosa ET and Malik A (2022) Enhanced weathering potentials—the role of in situ CO2 and grain size distribution. Front. Clim. 4:929268. doi: 10.3389/fclim.2022.929268

Beerling, D. J., Kantzas, E. P., Lomas, M. R., Wade, P., Eufrasio, R. M., Renforth, P., Sarkar, B., Andrews, M. G., James, R. H., Pearce, C. R., Mercure, J. F., Pollitt, H., Holden, P. B., Edwards, N. R., Khanna, M., Koh, L., Quegan, S., Pidgeon, N. F., Janssens, I. A., … Banwart, S. A. (2020). Potential for large-scale CO2 removal via enhanced rock weathering

with croplands. *Nature*, *583*(7815), 242–248. https://doi.org/10.1038/s41586-020-2448-9

Beerling, D. J., Leake, J. R., Long, S. P., Scholes, J. D., Ton, J., Nelson, P. N., Bird, M., Kantzas, E., Taylor, L. L., Sarkar, B., Kelland, M., Delucia, E., Kantola, I., Müller, C., Rau, G. H., & Hansen, J. (2018). Climate , Food and Soil Security. *Nature Plants*, *4*(March), 138–147. http://dx.doi.org/10.1038/s41477-018-0108-y

Bradford, M.A., Kuebbing, S. E., Polussa, A., Sanderman, J., Oldfield, E. E. (2025). Upstream data need to prove soil carbon as a climate solution. *Nature Climate Change*, 15:10, 1013-1016.

Buss, W., Hasemer, H., Ferguson, S., & Borevitz, J. (2024). Stabilisation of soil organic matter with rock dust partially counteracted by plants. Global Change Biology, 30, e17052. https://doi.org/10.1111/gcb.17052

Buss, W., Hasemer, H., Sokol, N.W. et al. Applying minerals to soil to draw down atmospheric carbon dioxide through synergistic organic and inorganic pathways. Commun Earth Environ 5, 602 (2024). https://doi.org/10.1038/s43247-024-01771-3

Cipolla, G., Calabrese, S., Noto, L. V., & Porporato, A. (2021). The role of hydrology on enhanced weathering for carbon sequestration II. From hydroclimatic scenarios to carbon-sequestration efficiencies. *Advances in Water Resources*, *154*(May), 103949. https://doi.org/10.1016/j.advwatres.2021.103949

Clobert, J., Chanzy, A., Galliard, J. Le, Chabbi, A., Greiveldinger, L., Caquet, T., Loreau, M., & Mougin, C. (2018). How to Integrate Experimental Research Approaches in Ecological and Environmental Studies : AnaEE France as an Example. *Frontiers in Ecology and Evolution*, *6*(April). https://doi.org/10.3389/fevo.2018.00043

Coplen, T. . (2011). Guidelines and recommended terms for expression of stable-isotope-ratio and gas-ratio measurement results. *Rapid Commun. Mass Spectrom.*, *25*, 2538–2560. https://doi.org/https ://doi.org/10.1002/rcm.5129

Cotrufo, M. F., Wallenstein, M. D., & Boot, C. M. (2013). *The Microbial Efficiency-Matrix Stabilization (MEMS) framework integrates plant litter decomposition with soil organic matter stabilization : do labile plant inputs form stable soil organic matter ?* 988–995. https://doi.org/10.1111/gcb.12113

Dietzen, C., Harrison, R., & Michelsen-Correa S., 2019. Effectiveness of enhanced mineral weathering as a carbon sequestration tool and alternative to agricultural lime: An incubation experiment. *International Journal of Greenhouse Gas Control*, *74(July 2018), pp251-258.* https://doi.org/10.1016/j.ijggc.2018.05.007

Dietzen, C., & Rosing, M. T. (2023). Quantification of CO2 uptake by enhanced weathering of silicate minerals applied to acidic soils. *International Journal of Greenhouse Gas Control*, *125*(June 2022), 103872. https://doi.org/10.1016/j.ijggc.2023.103872

Gadd, G. M., Rhee, Y. J., Stephenson, K., & Wei, Z. (2012). Geomycology: Metals, actinides and biominerals. *Environmental Microbiology Reports*, *4*(3), 270–296. https://doi.org/10.1111/j.1758-2229.2011.00283.x

Gao, K., Yu, Y.F., Xia, Z.T. et al. Response of height, dry matter accumulation and partitioning of oat (Avena sativa L.) to planting density and nitrogen in Horqin Sandy Land. Sci Rep 9, 7961 (2019). https://doi.org/10.1038/s41598-019-44501-y

Grolemund, G., & Wickham, H. (2011). Dates and Times Made Easy with lubridate. *Journal of Statistical Software*, *40*(3), 1–25. https://www.jstatsoft.org/v40/i03/

Gunning, P. J., Hills, C. D. & Carey, P. J. (2010). Accelerated carbonation treatment of industrial wastes. *Waste Management*. 30, 1081–1090.

Guo, F., Wang, Y., Zhu, H., Zhang, C., Sun, H., Fang, Z., Yang, J., Zhang, L., Mu, Y., Man, Y. B., & Wu, F. (2023). Crop productivity and soil inorganic carbon change mediated by enhanced rock weathering in farmland: A comparative field analysis of multi-agroclimatic regions in central China. *Agricultural Systems*, *210*(May), 103691. https://doi.org/10.1016/j.agsy.2023.103691

Hannes, M., Wollschläger, U., Schrader, F., Durner, W., Gebler, S., Pütz, T., Fank, J., Von Unold, G., & Vogel, H. J. (2015). A comprehensive filtering scheme for high-resolution estimation of the water balance components from high-precision lysimeters. *Hydrology and Earth System Sciences*, *19*(8), 3405–3418. https://doi.org/10.5194/hess-19-3405-2015

Holzer, I. O., Nocco, M. A., & Houlton, B. Z. (2023). Direct evidence for atmospheric carbon dioxide removal via enhanced weathering in cropland soil. *Environmental Research Communications*, *5*(10). https://doi.org/10.1088/2515-7620/acfd89

IPCC. (2014). Climate Change 2014 Synthesis Report: Summary Chapter for Policymakers. *Ipcc*, 31. https://doi.org/10.1017/CBO9781107415324

Kallenbach, C., & Grandy, A. S. (2011). Controls over soil microbial biomass responses to carbon amendments in agricultural

systems : A meta-analysis. *"Agriculture, Ecosystems and Environment," 144*(1), 241–252. https://doi.org/10.1016/j.agee.2011.08.020

Kantola, I. B., Blanc-Betes, E., Masters, M. D., Chang, E., Marklein, A., Moore, C. E., von Haden, A., Bernacchi, C. J., Wolf, A., Epihov, D. Z., Beerling, D. J., & DeLucia, E. H. (2023). Improved net carbon budgets in the US Midwest through direct measured impacts of enhanced weathering. *Global Change Biology*, *May*, 7012–7028. https://doi.org/10.1111/gcb.16903

Kelland ME, Wade PW, Lewis AL, et al. Increased yield and CO2 sequestration potential with the C4 cereal Sorghum bicolor cultivated in basaltic rock dust-amended agricultural soil. Glob Change Biol. 2020; 26: 3658–3676. https://doi.org/10.1111/gcb.15089

Kimball BA, 2016. Crop responses to elevated CO2 and interactions with H2O, N, and temperature. *Current Opinion in Plant Biology, 31:36-43.* https://doi.org/10.1016/j.pbi.2016.03.006

Li, J., Mavrodi, D. V., & Dong, Y. (2020). Effect of rock dust-amended compost on the soil properties, soil microbial activity, and fruit production in an apple orchard from the Jiangsu province of China. Archives of Agronomy and Soil Science, 67(10), 1313–1326. https://doi.org/10.1080/03650340.2020.1795136

McKinney, C. R., McCrea, J. M., Epstein, S., Allen, H. A., & Urey, H. C. (1950). Improvements in mass spectrometers for the measurement of small differences in isotope abundance ratios. *Rev. Sci. Instrum.*, *21*, 724–730. https://doi.org/https ://doi.org/10.1063/1.17456 98

Minasny, B., Malone, B. P., McBratney, A. B., Angers, D. A., Arrouays, D., Chambers, A., Chaplot, V., Chen, Z. S., Cheng, K., Das, B. S., Field, D. J., Gimona, A., Hedley, C. B., Hong, S. Y., Mandal, B., Marchant, B. P., Martin, M., McConkey, B. G., Mulder, V. L., … Winowiecki, L. (2017). Soil carbon 4 per mille. *Geoderma*, *292*, 59–86. https://doi.org/10.1016/j.geoderma.2017.01.002

Oksanen, J., Blanchet, F. G., Kindt, R., Legendre, P., Minchin, P. R., O'Hara, R. B., Simpson, G. L., Solymos, P., Henry, M., Stevens, H., & Wagner, H. (2013). *Vegan: Community Ecology Package. R package version 2.0-10.*

Peters, A., Groh, J., Schrader, F., Durner, W., Vereecken, H., & Pütz, T. (2017). Towards an unbiased filter routine to determine precipitation and evapotranspiration from high precision lysimeter measurements. *Journal of Hydrology*, *549*, 731–740.

https://doi.org/10.1016/j.jhydrol.2017.04.015

Pinheiro, J., Bates, D., & R coreTeam. (2023). *nlme: Linear and Nonlinear Mixed Effects Models* (p. R package version 3.1-162, https://CRAN.R-project.).

R core team. (2019). *R: A language and environment for statistical computing*. R Foundation for Statistical Computing. https://www.r-project.org/.

Ramos, C. G., Hower, J. C., Blanco, E., Oliveira, M. L. S., & Theodoro, S. H. (2022). Possibilities of using silicate rock powder: An overview. *Geoscience Frontiers*, *13*(1), 101185. https://doi.org/10.1016/j.gsf.2021.101185

Rijnders, J., Vicca, S., Struyf, E., Amann, T., Hartmann, J., Meire, P., Janssens, I., & Schoelynck, J. (2023). The effects of dunite fertilization on growth and elemental composition of barley and wheat differ with dunite grain size and rainfall regimes. *Frontiers in Environmental Science*, *11*(August), 1–19. https://doi.org/10.3389/fenvs.2023.1172621

Rineau, F., Groh, J., Claes, J., Grosjean, K., Mench, M., Moreno-druet, M., Povilaitis, V., Pütz, T., Szulc, W., Thijs, S., Vandenborght, J., Vangronsveld, J., Vereecken, H., Verhaege, K., Zydelis, R., & Loit, E. (2024). Limited effects of crop foliar Si fertilization on a marginal soil under a future climate scenario. *Heliyon*, *10*(December 2023), 1–12. https://doi.org/10.1016/j.heliyon.2023.e23882

Rineau, F., Malina, R., Beenaerts, N., Arnauts, N., Bardgett, R. D., Berg, M. P., Boerema, A., Bruckers, L., Clerinx, J., Davin, E. L., De Boeck, H. J., De Dobbelaer, T., Dondini, M., De Laender, F., Ellers, J., Franken, O., Gilbert, L., Gudmundsson, L., Janssens, I. A., … Vangronsveld, J. (2019). Towards more predictive and interdisciplinary climate change ecosystem experiments. *Nature Climate Change*, *9*(11), 809–816. https://doi.org/10.1038/s41558-019-0609-3

Roy, J., Rineau, F., De Boeck, H. J., Nijs, I., Pütz, T., Abiven, S., Arnone, J. A., Barton, C. V. M., Beenaerts, N., Brüggemann, N., Dainese, M., Domisch, T., Eisenhauer, N., Garré, S., Gebler, A., Ghirardo, A., Jasoni, R. L., Kowalchuk, G., Landais, D., … Milcu, A. (2021). Ecotrons: Powerful and versatile ecosystem analysers for ecology, agronomy and environmental science. *Global Change Biology*, *Online first*, 1–21. https://doi.org/10.1111/gcb.15471

Smith, P. (2004). How long before a change in soil organic carbon can be detected? *Global Change Biology*, 10, 1878–1883, doi: 10.1111/j.1365-2486.2004.00854.x

Sun, Z., Wu, S., Zhu, B., Zhang, Y., Bol, R., Chen, Q., & Meng, F. (2019). *Variation of 13 C and 15 N enrichments in different*

plant components of labeled winter wheat (Triticum aestivum L .). 1–22. https://doi.org/10.7717/peerj.7738

Swoboda, P., Döring, T. F., & Hamer, M. (2022). Remineralizing soils? The agricultural usage of silicate rock powders: A review. *Science of the Total Environment*, *807*. https://doi.org/10.1016/j.scitotenv.2021.150976

Vanderkelen, I., Zschleischler, J., Gudmundsson, L., Keuler, K., Rineau, F., Beenaerts, N., Vangronsveld, J., & Thiery, W. (2019). A new approach for assessing climate change impacts in ecotron experiments. *Biogeosciences Discussions*, 1–38. https://doi.org/10.5194/bg-2019-267

Vienne, A., Poblador, S., Portillo-Estrada, M., Hartmann, J., Ijiehon, S., Wade, P., & Vicca, S. (2022). Enhanced Weathering Using Basalt Rock Powder: Carbon Sequestration, Co-benefits and Risks in a Mesocosm Study With Solanum tuberosum. *Frontiers in Climate*, *4*(May), 1–14. https://doi.org/10.3389/fclim.2022.869456

Wickham, H., François, R., Henry, L., Müller, K., & Vaughan, D. (2023). *dplyr: A Grammar of Data Manipulation* (p. https://github.com/tidyverse/dplyr).